

Chapter 5 – Materials

5.1 Impurities.

The ingredients thought to play a role in the radiation hardness of silicon detectors are oxygen, carbon and tin. This hypothesis relies on the interpretation of experimental results and on defect kinetics models developed to explain the radiation induced changes in silicon detectors. Experimental results obtained from proton irradiation of epitaxial diodes exhibited better radiation tolerance than standard FZ silicon [5.1, 5.3]. A noticeable difference between epitaxial and standard silicon is the content of carbon and oxygen, suggesting the possible influence of these elements on the radiation hardness. The identification of some final defects (Table 3.2) and the models to explain their formation by reaction with primary induced defects support the hypothesis about the role of these impurities. The defects responsible for the changes in silicon are vacancy related. Possible candidates are divacancy (V_2) or multi-vacancy related defects (V_2O , V_3O , V_n with $n > 2$) [5.4-5.6]. An impurity suitable to improve the radiation tolerance of silicon detectors should act as a sink for vacancies and create electrically inactive complexes.

The role of oxygen is envisaged if the defects responsible for the changes in silicon are of the type V_nO , with $n > 1$. The formation of the divacancy and multi-vacancy oxygen complexes could be suppressed by a large O concentration, by enhancing the formation of the VO and limiting the V_2O , and therefore the V_nO , formation [5.5].

Another element found to act as a V sink is Sn. Experimental results on Sn enriched silicon material exhibited strong suppression of V_2 production [5.3].

Also phosphorus is an effective V sink. The ratio of the capture radius of V between P and O is about 14 [5.7]. P is a dopant in silicon, therefore it cannot be introduced in large concentration to avoid the drop of the resistivity. A possible solution is to introduce P in interstitial position (P_i), where it is not electrically active. A method is suggested below to introduce P_i in silicon.

Here are described some techniques used for the measurement of the impurity concentrations and the techniques to introduce impurities in the silicon ingot or in the silicon wafers.

5.1.1 Measurement techniques of the impurity concentration

Various methods can be used to measure the concentration of an impurity in the silicon crystal. Fourier Transform Infrared Spectroscopy (FTIR) at room temperature or at low temperature (5K) and Secondary Ion Mass Spectrometry (SIMS) are used to measure the content of O, C, Sn, B and P in our samples.

The infrared spectroscopy is a non-destructive technique that provides the average concentration of a particular impurity in a silicon sample. The intensity of the light passing through the sample is measured as a function of the light wavelength. Different impurities absorb different wavelengths, at a rate depending on the impurity content of the sample. The absorbed fraction is defined as absorbance $A = \log(I_0/I)$, where I_0 is the initial and I the transmitted light intensity. From the absorption spectrum, it is possible to isolate the peaks due to various impurities. The impurity concentrations are obtained by the comparison between the absorption peaks of the sample under measurement and a sample with known concentration of impurities.

FTIR is sensitive to interstitial oxygen (O_i) and interstitial (low temperature FTIR only) and substitutional carbon. The sensitivity depends on the thickness of the sample. O_i concentration can be measured down to $5 \cdot 10^{15} \text{ cm}^{-3}$ also on 300 μm thick samples by FTIR at 5K, and carbon can be measured only on 1-2 mm thick samples with a sensitivity of $\approx 5 \cdot 10^{15} \text{ cm}^{-3}$.

For SIMS, a beam of accelerated primary ions (1-20 keV) is focused on the surface of the sample under measurement inside an ultrahigh vacuum box. The impact of the impinging ions on the sample causes sputtering of surface atoms or molecules from the material examined. Some of the sputtering species are ionised and are called secondary ions. They are analysed with a mass spectrometer. The concentration of the different species is calculated by comparison with reference samples with known concentration of impurities, measured in identical conditions as the one under examination. The primary ions used are usually O_2^+ , O^+ , Ar^+ or Cs^+ . The choice of the primary ion type and rate depends on the required analysis. SIMS measurements can be performed at a single point (bulk measurement) or by a dynamic profiling technique, which provides the impurity concentration as a function of the depth.

The sensitivity limit in the case of bulk measurement by SIMS technique is $\approx 5 \cdot 10^{16} \text{ cm}^{-3}$ for oxygen, $\approx 5 \cdot 10^{15} \text{ cm}^{-3}$ for carbon and $\approx 1 \cdot 10^{16} \text{ cm}^{-3}$ for tin. The limit for the concentration profile is $\approx 1 \cdot 10^{16} \text{ cm}^{-3}$ for carbon and $1-1.5 \cdot 10^{17} \text{ cm}^{-3}$ for oxygen. SIMS is sensitive to the overall concentration of a given impurity, for example oxygen, irrespectively to the atom position or binding in the crystal (interstitial, substitutional or SiO_2 precipitate). The position of the atom is important for the possible reaction with radiation induced defects [5.8]. Therefore, it is often useful to combine results from both, SIMS and FTIR techniques.

FTIR measurements were performed at University of Gent [5.9] (low and room temperature), at the Czech Technical University of Prague [5.10] and at ITME [5.11]. SIMS measurements were performed by EVANS Company [5.12].

5.1.2 Introduction of impurities in the silicon ingot

A successful enrichment of silicon implies a final concentration of a particular impurity significantly higher than the one met in the standard silicon material and a uniform distribution of the impurity.

The impurities can be introduced during the ingot production or into the silicon wafer.

The deliberate introduction of impurities in the silicon ingot is achieved through diffusion in the FZ region from gaseous or solid impurity sources. A suitable gas containing the diffusing species is fluxed on the melting silicon during the FZ refinement. The impurities penetrate and diffuse into the melt. Several parameters have to be taken into account, as for example the flux rate, gas pressure, segregation coefficient of the particular impurity between the liquid and the solid silicon and pulling rate of the heater.

The solid sources of the diffusing species are obtained by drilling holes into the polysilicon rod and filling them with the impurity or interposing a highly doped silicon piece (e.g. highly carbonate CZ silicon) between the crystal seed and the polysilicon rod. The FZ refinement allows the diffusion of the impurities from the solid source into the silicon ingot. The parameters to be adjusted, in order to obtain the required concentration and homogeneity, are the amount and the initial distribution of the impurity and the pulling rate of the heater.

5.1.3 The impurity diffusion experiment

The high temperature diffusion was proposed and developed to introduce impurities inside the silicon wafer instead of the ingot.

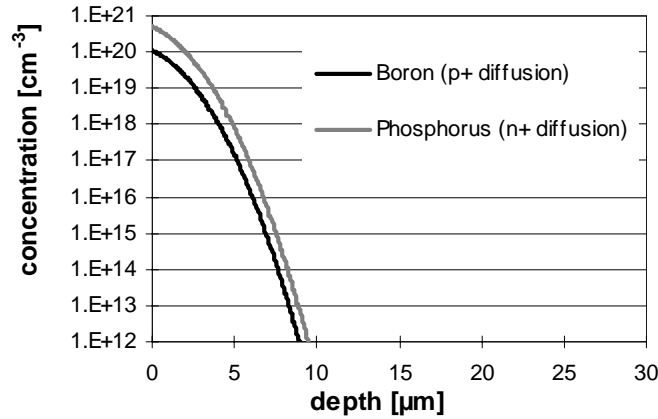


Fig. 5.1 Calculated diffusion profile of P and B for diffusion during 3h at 1200°C.

The diffusion technique is used to form the junction and the ohmic contact, as mentioned in § 2.3.2 for the mesa diode production. B and P diffuse from a paper source during 4 hours at 1200 °C. The expression for the diffusion coefficient, D , as a function of the temperature is [2.7]:

$$D(T) = D_0 \exp\left(-\frac{E_d}{k_B T}\right) \quad (5.1)$$

where D_0 is the apparent value of the diffusion coefficient at infinite temperature and E_d is an activation energy. Table 5.1 lists the diffusion parameters for P and B found by several workers [5.13]. There is a noticeable spread between the given values, which reflects the dependence of the diffusion process on parameters other than temperature. In fact, the background impurity concentration and the crystal quality (density of vacancies and interstitials in damaged regions) influence the microscopic mobility. In that sense, the evaluation of the diffusion parameters must be performed in a particular case with reproducible conditions. Figure 5.1 shows the P and B profiles calculated using the diffusion coefficient $1.16 \cdot 10^{-12} \text{ cm}^2 \text{ s}^{-1}$ for phosphorus and $1.12 \cdot 10^{-12} \text{ cm}^2 \text{ s}^{-1}$ for boron on the basis of the diffusion theory

presented in Appendix B. The calculated depths of the B and P diffusion are $\approx 10 \mu\text{m}$ and represent the estimated depth of the junction and the ohmic contacts of mesa detectors.

Phosphorus diffusion parameters

E_a [eV]	D_0 [cm^2s^{-1}]	$D(1200 \text{ }^\circ\text{C})$ [cm^2s^{-1}]	$D(1300 \text{ }^\circ\text{C})$ [cm^2s^{-1}]
2.52	0.001	$2.39 \cdot 10^{-12}$	$8.45 \cdot 10^{-12}$
3.69	10.5	$2.5 \cdot 10^{-12}$	$1.58 \cdot 10^{-11}$
3.66	3.85	$7.25 \cdot 10^{-12}$	$1.16 \cdot 10^{-12}$
3.61	3.62	$1.62 \cdot 10^{-12}$	$9.86 \cdot 10^{-12}$
3.69	3.7	$8.8 \cdot 10^{-13}$	$5.58 \cdot 10^{-12}$
3.5	1.3	$1.38 \cdot 10^{-12}$	$7.97 \cdot 10^{-12}$
3.69	5.3	$1.26 \cdot 10^{-12}$	$8.0 \cdot 10^{-12}$
3.51	0.6	$5.89 \cdot 10^{-13}$	$3.42 \cdot 10^{-12}$

Boron diffusion parameters

E_a [eV]	D_0 [cm^2s^{-1}]	$D(1200 \text{ }^\circ\text{C})$ [cm^2s^{-1}]	$D(1300 \text{ }^\circ\text{C})$ [cm^2s^{-1}]
3.87	24	$1.38 \cdot 10^{-12}$	$9.6 \cdot 10^{-12}$
3.59	2.46	$1.29 \cdot 10^{-12}$	$7.76 \cdot 10^{-12}$
3.77	11.5	$1.46 \cdot 10^{-12}$	$9.62 \cdot 10^{-12}$
3.6	2.64	$1.28 \cdot 10^{-12}$	$7.74 \cdot 10^{-12}$
3.7	5.1	$1.12 \cdot 10^{-12}$	$7.15 \cdot 10^{-12}$
3.68	17.1	$4.4 \cdot 10^{-12}$	$2.78 \cdot 10^{-11}$
3.69	16	$3.81 \cdot 10^{-12}$	$2.41 \cdot 10^{-11}$

Phosphorus solubility [atoms cm^{-3}]	Boron solubility [atoms cm^{-3}]
$1.3 \cdot 10^{21}$ (1150 $^\circ\text{C}$)	$5 \cdot 10^{20}$ (1150 $^\circ\text{C}$)

Table 5.1 *Diffusion parameters for boron and phosphorus in silicon found by different workers [5.13].*

The junction depth can be measured by profiling the resistivity. Figure 5.2 shows the P (ohmic side) and B (junction side) concentrations versus depth measured by the Czech Technical University of Prague using the spreading resistance method. This result confirms that the depth of the diffusions is $\geq 10 \mu\text{m}$.

A singular result has been obtained profiling the P and B concentration by SIMS. The B concentration in the junction side, shown in Fig. 5.3(a), exhibits a profile which reproduces the expected depth of the junction ($\approx 13 \mu\text{m}$) but still shows a very high level in the bulk ($9 \cdot 10^{16} \text{ cm}^{-3}$ at $60 \mu\text{m}$). More surprising, the P concentration is 5 orders of magnitude larger than the level given by the silicon manufacturer and found by C-V and CCE measurements ($\approx 1 \cdot 10^{12} \text{ at. cm}^{-3}$). The P profile in the ohmic side, shown in Fig. 5.3(b), agrees with the expected depth of

the ohmic contact ($\approx 15 \mu\text{m}$) but shows a high concentration level into the bulk as for the

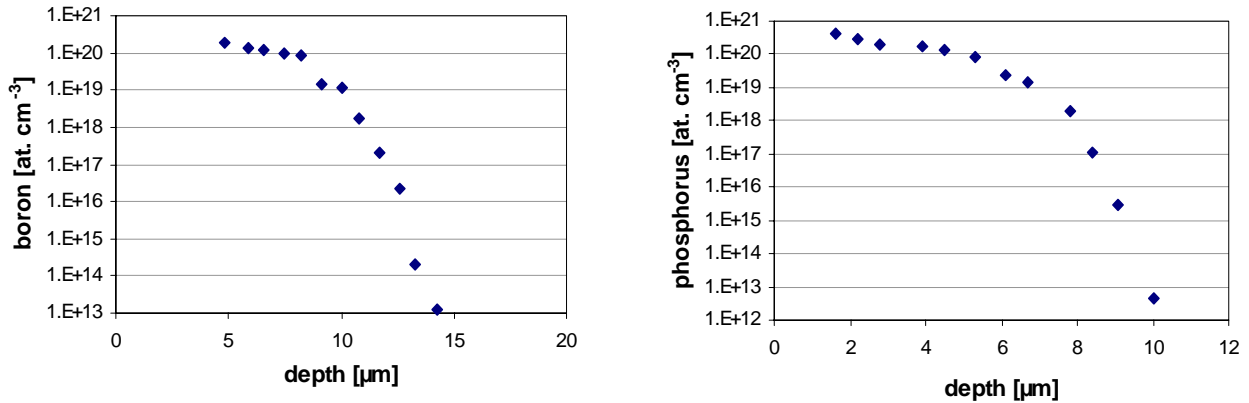


Fig. 5.2 *Boron and phosphorus concentrations versus depth in a mesa diode, measured by the spreading resistance method.*

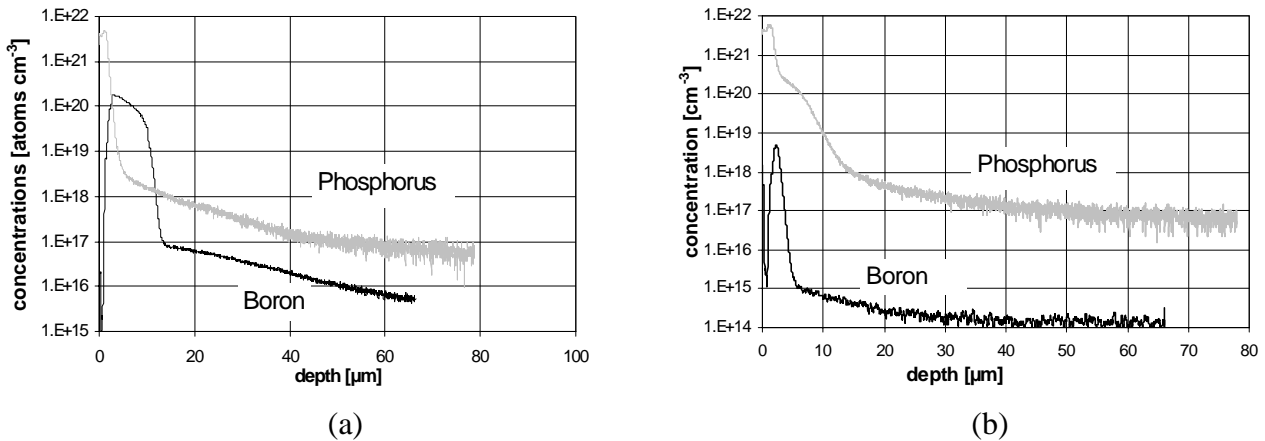


Fig. 5.3 *Phosphorus and boron profiles obtained by SIMS from a mesa sample: (a) junction (p^+) side (b) ohmic (n^+) side.*

The P doping contributes to the resistivity only if phosphorus atoms are in substitutional positions. A possible explanation for the high P concentration is that only a small fraction of the phosphorus is activated. In order to test this hypothesis, some mesa diodes were annealed by ITME to activate the phosphorus, in two successive steps of one hour at $800 \text{ }^\circ\text{C}$, in air and in H_2 atmosphere, after removing the metallic contacts. The resulting bulk resistivity profiles are shown in Fig. 5.4. The resistivity is found to increase after the annealing steps, instead of decreasing as expected from the activation of a large amount of phosphorus. This result suggests that the dopants activated by the annealing treatment are acceptors compensating

partially the n-type doping level. The origin of the strong P (and, in a less extent B) SIMS signal is still unexplained.

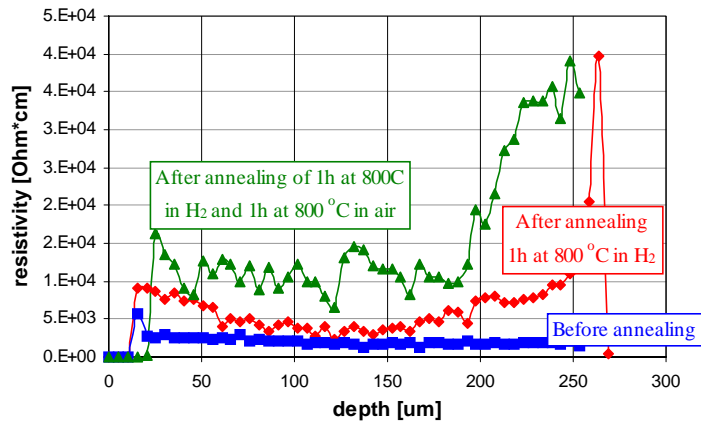


Fig. 5.4 Resistivity profile of a mesa diode before and after two successive annealing steps of 1 h at 800 °C in H_2 and normal atmosphere. Measurements performed by ITME.

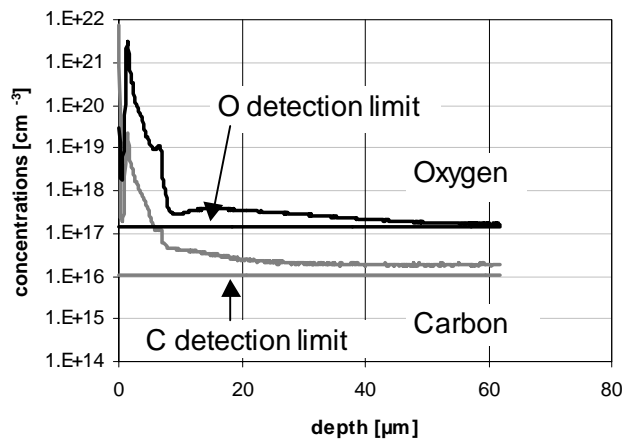


Fig. 5.5 Oxygen and carbon SIMS profiles in a mesa diode.

The high temperature diffusion of P and B in mesa diodes is performed in normal air atmosphere from appropriate paper sheets. Oxygen and carbon also diffuse into the diode during these annealing steps and their concentration profiles, measured by SIMS up to 60 μm are shown in Fig. 5.5. The paper, atmosphere and dissolution of the unknown B and P compounds used as diffusion sources provide the diffusing atoms.

These results demonstrate that the diffusion is an effective method to introduce some kind of impurities into the silicon wafer.

Table 5.2 lists the diffusion parameters for O, C and Sn. Figure 5.6 shows the calculated concentration profile at various temperatures and times for C and Sn.

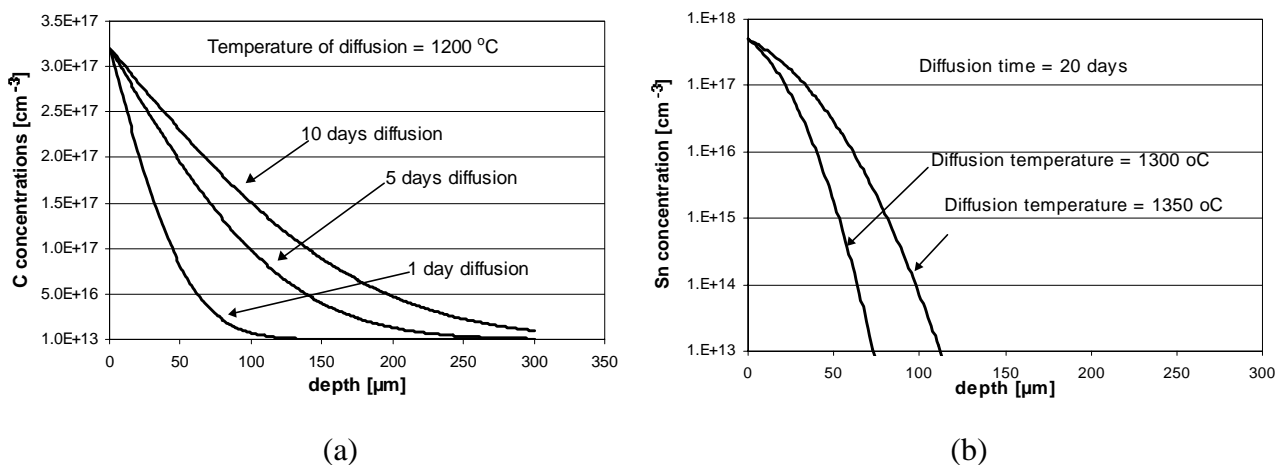


Fig. 5.6 Calculated concentration profiles for (a) C and (b) Sn in silicon for different temperatures and times.

A significant concentration of carbon up to the middle of the wafer bulk (150μm) can be achieved during ≥ 5 days at 1200 °C. The diffusion time to reach a significant tin concentration is prohibitive. O is the faster diffuser between the considered impurities. We envisaged the high temperature O diffusion from a layer of SiO₂ grown on the wafer surface.

The oxygen diffusion tests have been performed at the Technion University in Haifa (Israel) using 1x1 cm² and 300 μm thick samples of standard silicon produced by POLOVODICE. Layers of ≈ 3000 Å of local oxide were grown on both sides by the dry oxidation technique. The samples, then, were heated to 1150 °C in a N₂ atmosphere to allow desorption of oxygen from the SiO₂ at the interface and its diffusion into the bulk.

Oxygen diffusion parameters			
E _d [eV]	D ₀ [cm ² s ⁻¹]	D(1150 °C) [cm ² s ⁻¹]	D(1200 °C) [cm ² s ⁻¹]
3.5	135	$5.44 \cdot 10^{-11}$	$1.43 \cdot 10^{-10}$
2.55	0.21	$1.96 \cdot 10^{-10}$	$3.97 \cdot 10^{-10}$
3.5	83	$3.35 \cdot 10^{-11}$	$8.82 \cdot 10^{-10}$
2.4	0.091	$2.88 \cdot 10^{-10}$	$5.60 \cdot 10^{-10}$
3.15	22.6	$1.58 \cdot 10^{-10}$	$3.78 \cdot 10^{-10}$
2.44	0.07	$1.60 \cdot 10^{-10}$	$3.15 \cdot 10^{-10}$
2.77	1.5	$2.33 \cdot 10^{-10}$	$5.01 \cdot 10^{-10}$
2.54	0.17	$1.72 \cdot 10^{-10}$	$3.47 \cdot 10^{-10}$

2.51	0.11	$1.42 \cdot 10^{-10}$	$2.85 \cdot 10^{-10}$
2.43	0.033	$8.19 \cdot 10^{-11}$	$1.60 \cdot 10^{-10}$
2.53	0.14	$1.54 \cdot 10^{-10}$	$3.10 \cdot 10^{-10}$

Carbon diffusion parameters			
2.92	0.33	$1.51 \cdot 10^{-11}$	$3.38 \cdot 10^{-11}$

Tin diffusion parameters			
D(1200 °C) [cm ² s ⁻¹]	D(1250 °C) [cm ² s ⁻¹]	D(1300 °C) [cm ² s ⁻¹]	D(1350 °C) [cm ² s ⁻¹]
$\approx 1 \cdot 10^{-13}$	$\approx 3 \cdot 10^{-13}$	$\approx 8.5 \cdot 10^{-13}$	$\approx 2 \cdot 10^{-12}$

Oxygen solubility [atoms cm ⁻³]	Carbon solubility [atoms cm ⁻³]	Tin solubility [atoms cm ⁻³]
$\approx 8.4 \cdot 10^{17}$ (1250 °C)	$\approx 1.5 \cdot 10^{18}$ (1400 °C)	$> 10^{20}$ [5.22]

Table 5.2 Diffusion parameters and solubility for O, C and Sn in silicon [5.13].

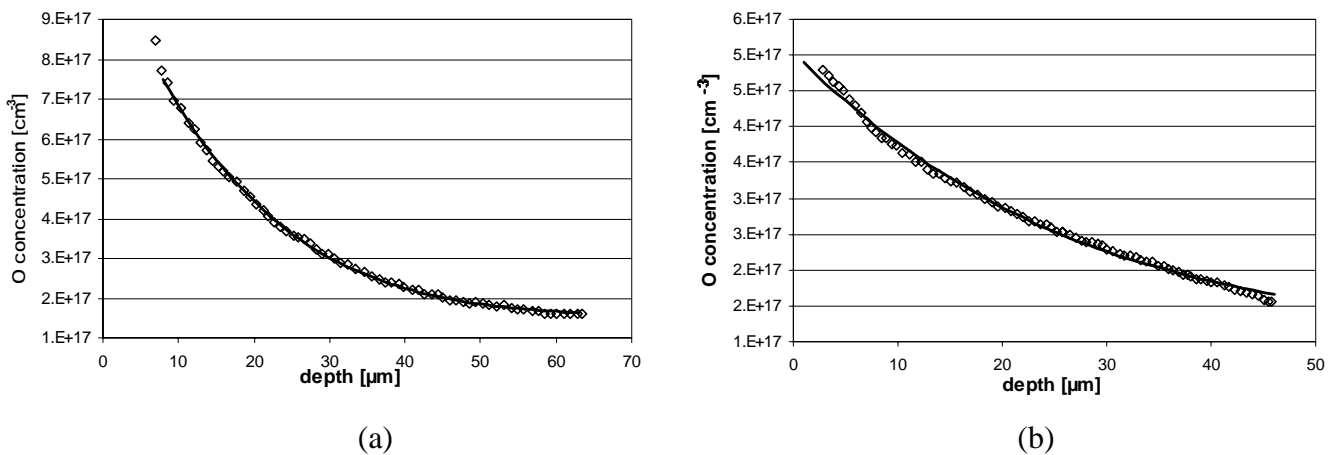


Fig. 5.7 Oxygen profile in (a) a mesa detector (3h at 1200 °C) and (b) a sample diffused at Technion (20h at 1150 °C).

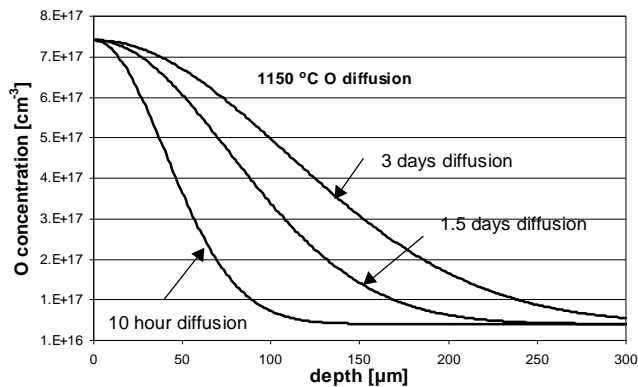


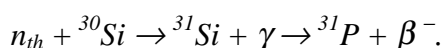
Fig. 5.8 Calculated oxygen profile for different diffusion time at 1150 °C.

The O concentration was profiled by SIMS. Figure 5.7(a) shows the measured O profile for a mesa diode diffused at DIOTEC in normal air atmosphere up to $\approx 60 \mu\text{m}$, and Fig. 5.7(b) shows a similar profile for a sample diffused at Technion. The fits have been performed using eq. C.13. The diffusion coefficient value resulting from the fit is $2.25 \cdot 10^{-10} \text{ cm}^2 \text{ s}^{-1}$ for the diffusion at Technion (1150 °C) and $8.96 \cdot 10^{-10} \text{ cm}^2 \text{ s}^{-1}$ for the diffusion during the mesa process (1200 °C). The diffusion conditions at Technion (O source, N₂ atmosphere and temperature cycle) are well controlled and therefore this process is more reproducible. Figure 5.8 shows the predicted O profile for three different diffusion times.

5.1.4 Neutron transmutation doping of silicon

The neutron transmutation doping (NTD) of silicon uses the reaction of thermal neutron with silicon atoms to produce high resistivity n-type silicon from starting p-type material [2.4, 5.14].

The reaction is:



The silicon atom goes in interstitial position because of the recoil during the gamma emission, and the phosphorus is produced in an interstitial site (P_i). The relationship between the generated P concentration, N_P , and the thermal neutron fluence, Φ_{th} , is expressed by:

$$N_P = K\Phi_{th} \quad (5.2)$$

where K is the transmutation constant. The value of K is $\approx 1.7 \cdot 10^{-4} \text{ cm}^{-1}$ [5.14]. The interstitial phosphorus is activated (pushed in substitutional position) by heating the silicon at $\approx 850 \text{ °C}$ during two hours.

It is possible to introduce P_i in a silicon detector positioning the sample in a thermal neutron flux. To achieve a significant P_i concentration, the total fluence of thermal neutron is very high: $\approx 6 \cdot 10^{20} \text{ n}_{th} \text{ cm}^{-2}$ are required to obtain $\approx 10^{17} \text{ P}_i \text{ cm}^{-3}$.

The more powerful sources of n_{th} are nuclear reactors, but the contribution of fast neutron in reactors is on the order of 10^{-3} - 10^{-4} times the n_{th} flux. Considering the value of K , the fluence of fast neutrons suffered by a detector doped in a nuclear reactor is very high: roughly, one damaging particle hit the detector for each P_i created.

5.2 Overview of the materials

Four manufacturers produced the tested materials: WACKER [5.15], POLOVODICE [5.16], ITME [5.12] AND MACOM [5.17]. Table 5.3 lists the materials, indicating the concentration of the important impurities, the impurity introduction technique and the resistivity. The standard FZ materials, with different resistivities, have been produced by WACKER (#1, #2, #3) and POLOVODICE (#4, #5). Material #5 has been used as a reference. The impurity concentration indicated in Table 5.3 for some of the standard materials are in the limit of the FZ silicon [2.4].

Materials #6 and #7 are enriched by O and C by gaseous and solid diffusion respectively. Their final concentration is only between 4 to 10 times the concentration of the standard silicon. Materials #8, #9 and #10 are standard POLOVODICE silicon wafers with additional oxygen introduced by the high temperature diffusion method, as described above. The diffusion was performed in ITE [5.18] during 24, 48 and 72 hours at 1150 °C. The resulting O and C concentration profiles are shown in Fig. 5.9 as measured by SIMS. The O_i concentration, measured by FTIR, is $\geq 1 \cdot 10^{17} \text{ cm}^{-3}$. The O and O_i concentrations are then ≥ 100 and ≥ 50

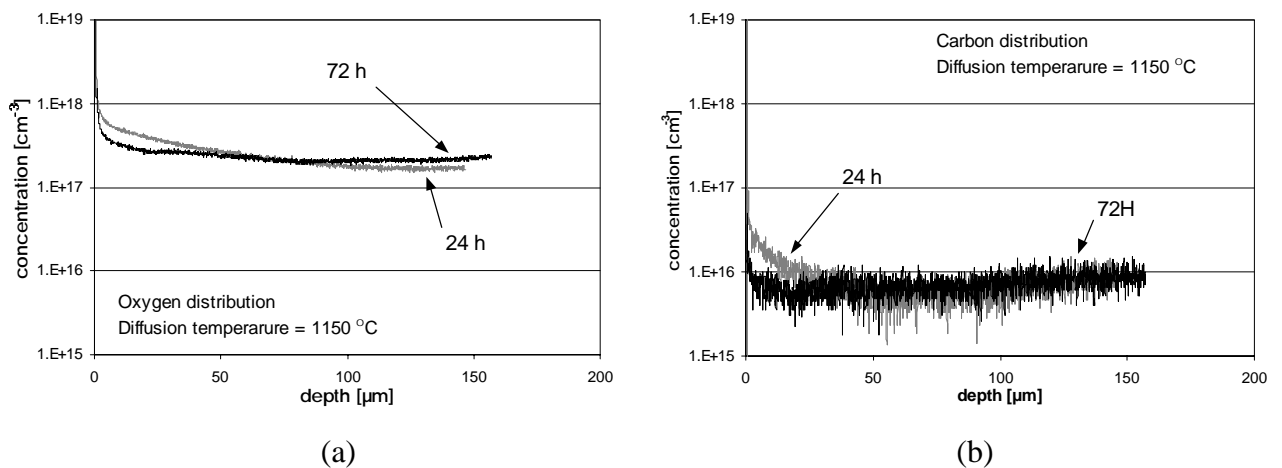


Fig. 5.9 SIMS profile of (a) O and (b) C concentration in O-diffused wafers #8 and #10.

times larger than the concentration in standard FZ silicon, respectively.

Materials #11 and #12 are O-enriched by the jet diffusion technique developed by ITME. O is incorporated in silicon spraying a gas of Ar and O₂ on the melting zone. The distance of the gas-pipe outlet from the melt and the gas flow rate were optimised experimentally [5.19].

Material #13, produced by ITME, is enriched with tin (Si:Sn) up to the concentration of $1.8 \cdot 10^{17} \text{ cm}^{-3}$. The expected resistivity from the polysilicon rod was $\approx 1000 \ \Omega \text{ cm}$. The actual resistivity after the FZ refinement is $\approx 210 \ \Omega \text{ cm}$. Tin introduces a donor ($E_c - 0.25 \text{ eV}$) and an acceptor ($E_v + 0.27 \text{ eV}$) levels in silicon [5.20, 2.1]. Considering the donor level as dominant, the ionised fraction of tin ($N_{D,Sn}$) corresponds to:

$$N_{D,Sn} \approx N_{Sn} \exp\left(-\frac{0.25}{k_B T}\right) \approx 9.2 \cdot 10^{12} \quad (5.3)$$

where N_{Sn} is the total concentration of tin. The corresponding value of the resistivity is $\approx 470 \ \Omega \text{ cm}$. This value is not far from the actual value and indicates that Sn in silicon acts as an effective donor.

The epitaxial materials #14 and #15 were produced by MACOM using different growth technique. The first material is a 100 μm thick epitaxial layer grown on a $\langle 111 \rangle$ CZ substrate, and the second is 150 μm thick, grown on a $\langle 100 \rangle$ CZ substrate. The manufacturer changed also other parameters of the growing technique between the first and the second materials, in order to achieve a thicker epitaxial layer. The details of the growth processes of the two productions are not available. It must be underline that the radiation hardness improvement exhibited by epitaxial diodes [5.2] was observed on diodes made from material #14. Figure 5.10 shows the oxygen and carbon concentration profiles measured by SIMS for material #14.

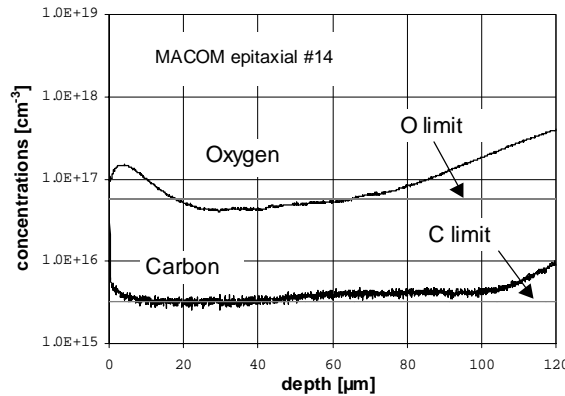


Fig. 5.10 Oxygen and carbon concentration profiles measured by SIMS for material #14.

Materials from #16 to #22 are n-type and p-type epitaxial silicon wafers 100, 150 and 200 μm thick produced by ITME. Material #17 was produced with a 0.5 $\mu\text{m}/\text{min}$ growing rate of the epitaxial layer, while the other epitaxial materials were grown at the rate of 1 $\mu\text{m}/\text{min}$. Figure 5.11 shows the oxygen and carbon concentration profiles measured by SIMS for some of these materials.

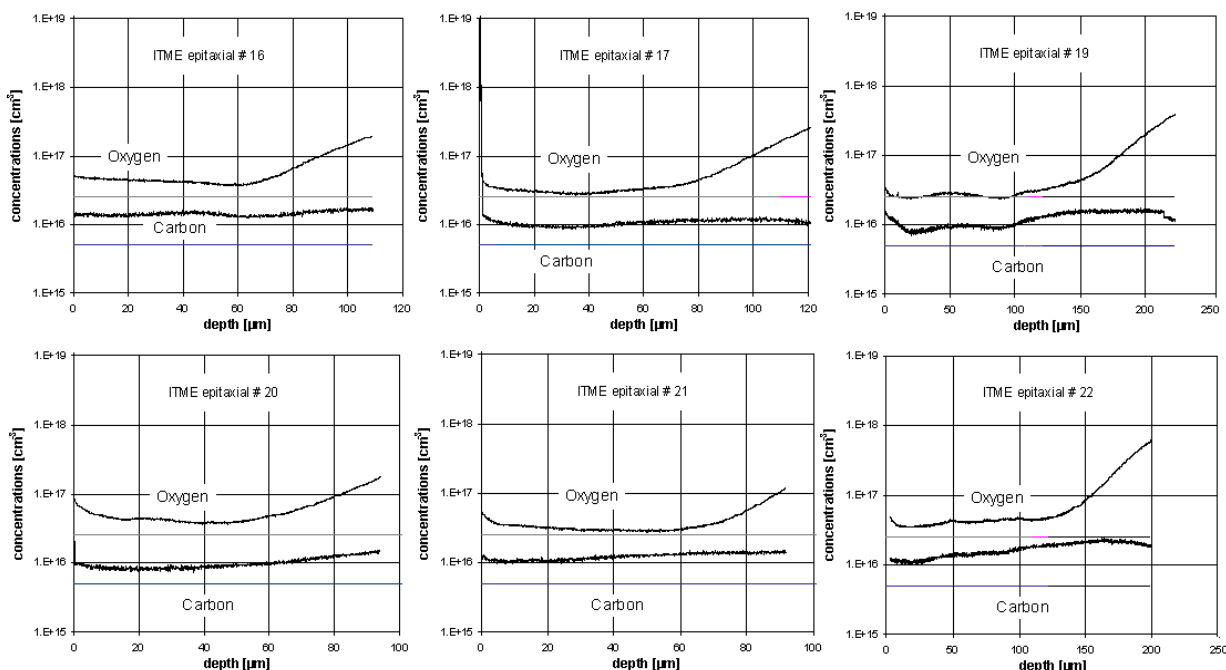


Fig. 5.11 *Oxygen and carbon concentration profiles measured by SIMS for various ITME epitaxial materials.*

Material #23 is NTD with resistivity of $\approx 3000 \Omega \text{ cm}$ produced by WACKER.

Standard planar diodes made from POLOVODICE silicon were submitted to a flux of thermal neutron [5.10], with a ratio $n_{th}/n_{fast} \approx 10^5$ (material #24). The final fluence of n_{th} was $\approx 1 \cdot 10^{13} \text{ cm}^{-2}$, then the P_i concentration is only $\approx 1.7 \cdot 10^9 \text{ cm}^{-3}$.

Hundreds of diodes have been produced from these materials using planar and mesa technologies. Several of them have been processed by both methods, allowing the estimate of the influence of the diode processing on the radiation hardness of the detectors.

5.3 Devices

The devices have been produced by CANBERRA [2.9], ITE [5.18], SINTEF [2.10] and DIOTEC [5.21]. CANBERRA and SINTEF use planar technology with implanted junction and ohmic contact. The implantation is performed by 60 keV B ions for the junction and by 150 keV P ions for the ohmic contact formation in n-type diodes. Figure 5.12 shows the depth of the B and P implantation calculated by the TRIM simulation package [4.10]. The peak concentration is $\approx 10^{19} \text{ cm}^{-3}$ for both implants.

ITE uses planar technology with diffused junction and ohmic contact. The junction of n-type diodes is fabricated by diffusion of B during 6 minutes at 1085 °C and 15 minutes at 950 °C. The junction depth is $\approx 0.6 \mu\text{m}$ and the surface B concentration is $\approx 1.2 \cdot 10^{15} \text{ cm}^{-3}$. The ohmic contact is fabricated by diffusion of P during 23 minutes at 1050 °C. The resulting depth is $\approx < 1 \mu\text{m}$ and the surface P concentration is $\approx 4 \cdot 10^{15} \text{ cm}^{-3}$.

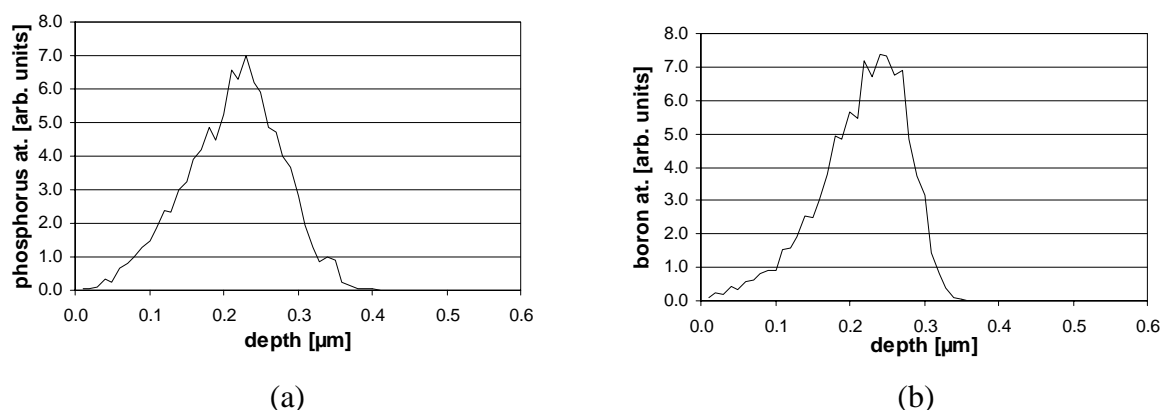


Fig. 5.12 *Simulated distribution of the implanted (a) P and (b) B ions for the ohmic and junction side formation in the planar process.*

DIOTEC fabricates diodes using the mesa technology. The diffusion process for the junction and the ohmic contact formation was described in § 5.1.3 and the resulting depths are 10-15 μm .

Manufacturer	ef #	Wafer type	Impurity introduction technique	Impurities			Resistivity [Ω cm]	Conductivity
				Oxygen [cm^{-3}]	Carbon [cm^{-3}]	Tin [cm^{-3}]		
WACKER	1	FZ std.					≈ 5000	n-type
WACKER	2	FZ std.					≈ 1500	n-type
WACKER	3	FZ std.					≈ 400	n-type
POLOVODICE	4	FZ std.					≈ 7000	n-type
POLOVODICE	5	FZ std.		$2 \cdot 10^{15}$ ^(a) (d)	$5 \cdot 10^{15}$ (a) (d)		≈ 2200	n-type
POLOVODICE	6	FZ + O	Gas diff. in FZ	$6.7 \cdot 10^{15}$ (a) (b) (d)	$9 \cdot 10^{15}$ (a) (d)		≈ 2200	n-type
POLOVODICE	7	FZ + C	Solid diff. in FZ				≈ 2200	n-type
POLOVODICE	8	FZ + O	24 h high T diffusion	$2.5 \cdot 10^{17}$ (c)	$7 \cdot 10^{15}$ (c)		≈ 2400	n-type
POLOVODICE	9	FZ + O	48 h high T diffusion	$2.5 \cdot 10^{17}$ (a) (b) (c)	$7 \cdot 10^{15}$ (c)		≈ 2400	n-type
POLOVODICE	10	FZ + O	72 h high T diffusion	$2.5 \cdot 10^{17}$ (c)	$7 \cdot 10^{15}$ (c)		≈ 2400	n-type
POLOVODICE	11	FZ + O	Jet diff. In FZ	$2.3 \cdot 10^{17}$ (a) (b) (c)	$1.2 \cdot 10^{16}$ (c)		≈ 750	n-type
POLOVODICE	12	FZ + O	Jet diff. In FZ	$1.4 \cdot 10^{17}$ (a)	$< 2 \cdot 10^{16}$ (a)		≈ 1200	n-type
POLOVODICE	13	FZ + Sn	Solid diff. In FZ	$6.2 \cdot 10^{16}$ (d)	$2.2 \cdot 10^{16}$ (d)	$1.8 \cdot 10^{17}$ (d)	≈ 210	n-type
MACOM	14	Epi. 100 μm	Substrate diffusion	$5 \cdot 10^{16}$ ^(c)	$3 \cdot 10^{15}$ ^(c)		≈ 550	n-type
MACOM	15	Epi. 150 μm	Substrate diffusion				≈ 2000	n-type
ITME	16	Epi. 100 μm	Substrate diffusion	$.5 \cdot 10^{16}$ ^(c)	$1.4 \cdot 10^{16}$ ^(c)		≈ 3000	n-type
ITME	17	Epi. 100 μm 0.5 $\mu\text{m}/\text{min}$.	Substrate diffusion	$.1 \cdot 10^{16}$ ^(c)	$1.0 \cdot 10^{16}$ ^(c)		≈ 3000	n-type
ITME	18	Epi. 150 μm	Substrate diffusion	$4 \cdot 10^{16}$ (c)	$1.2 \cdot 10^{16}$ ^(c)		≈ 6000	n-type
ITME	19	Epi. 200 μm	Substrate diffusion	$.5 \cdot 10^{16}$ ^(c)	$1.2 \cdot 10^{16}$ ^(c)		≈ 5500	n-type
ITME	20	Epi. 100 μm	Substrate diffusion	$.0 \cdot 10^{16}$ ^(c)	$1.0 \cdot 10^{16}$ ^(c)		≈ 500	p-type
ITME	21	Epi. 150 μm	Substrate diffusion	$.0 \cdot 10^{16}$ ^(c)	$1.2 \cdot 10^{16}$ ^(c)		≈ 700	p-type
ITME	22	Epi. 200 μm	Substrate diffusion	$.0 \cdot 10^{16}$ ^(c)	$1.5 \cdot 10^{16}$ ^(c)		≈ 1000	p-type
WACKER	23	FZ	NTD				≈ 3000	n-type
POLOVODICE	24	FZ	NTD				≈ 2200	n-type

Table 5.3 *Tested silicon materials. Labels (*) indicate the analysis method used for the impurity concentrations: ^(a) Fourier Transform Infrared Spectroscopy (FTIR) at room temperature, ^(b) FTIR at 5K, ^(c) Secondary Ion Mass Spectrometry (SIMS) profiling and ^(d) SIMS bulk measurement.*